Modeling the Response of Photoacoustic Gas Sensors

Samara L. Firebaugh*[1], Francois Roignant[2], and Eugene A. Terray[3]
[1]United States Naval Academy, [2]Polytechnique Nantes, [3]Woods Hole Oceanographic Institution
*Corresponding author: 105 Maryland Avenue, Mail Stop 14B, Annapolis, MD 21403, firebaug@usna.edu

Abstract: A fast, high-sensitivity detector is required for studies of environmentally relevant gases. Photoacoustic spectroscopy (PAS), an absorption spectroscopy technique in which absorption is detected as sound, is explored as a possible solution. A tuning-fork based PAS sensor is modeled using Comsol. The model combines the acoustic and piezoelectric modules and also includes viscous damping. The model results are consistent with published experimental results.

Keywords: photoacoustic spectroscopy, trace gas measurement, finite-element modeling, tuning fork, piezoelectric sensor

1. Introduction

Accurate measurements of the atmosphere-ocean fluxes of trace gases are important to an improved understanding of the cycling of climatically relevant gases in environmental studies. The direct eddy correlation (EC) method, which is considered to be the benchmark for accurate determination of air-sea fluxes of trace gases, relies on high-frequency measurements of the fluctuations of vertical wind velocity and gas concentration, and requires fast response sensors in combination with high sensitivity [1]. These twin requirements have precluded oceanographic use of the EC technique for many species of interest, and direct measurements have been limited mainly to carbon dioxide at relatively high flux levels.

Therefore, there is a need for a fast, highly sensitive, gas concentration sensor, that could be integrated with a sonic anemometer, motion sensing, and data acquisition into an EC flux package suitable for operation from buoys and other platforms, such as ships. Photoacoustic spectroscopy (PAS) is an attractive technique because it affords the possibility of compact, rugged sensors having concentration sensitivity in the parts-per-billion (ppb) range [2, 3].

PAS cells measure gas concentration through the collisional de-excitation of optically-excited molecules. This causes heating and produces a pressure perturbation in the gas, which can be sensed by various means. The earliest PAS sensors modulated the optical excitation at acoustic frequencies and used miniature electret microphones to detect the pressure wave. A further gain in sensitivity can be obtained by using a cell that is resonant at the acoustic frequency. For carbon dioxide, sensitivities in the range of parts-per-million can be realized by this approach. However parts-per-billion sensitivity requires improved detectors.

One approach, pioneered by a group at Rice University [4, 5] is to use a resonant quartz tuning fork (QTF) which, because of its high "Q-factor" (typically of order 10^4 at atmospheric temperature and pressure), is an extremely sensitive detector. Modeling the performance of such a device presents an interesting multiphysics problem. The system Q depends on viscous effects, the re-radiation of sound, and structural damping within the fork. In addition to this, one must include the structure of the acoustic field within the cell and the piezoelectric transduction of the mechanical signal to an electrical signal. Petra *et al.* [6] have developed an analytical model for the problem, but make several necessary simplifying assumptions, such as neglecting the reradiation of the acoustic field due to the tuning fork resonance. Numerical modeling is essential in order to fully test various design options at an acceptable cost.

2. Theory

The response in a tuning fork PAS cell can be broken down as follows:

(1) Laser light is incident on the cell and frequency modulated at half the mechanical resonance frequency, f_0, of the tuning fork.
(2) An absorption line in the gas is crossed twice during each modulation period. The

excited gas molecules relax the absorption energy through molecular collisions, locally heating the sample gas, and launching an acoustic wave at frequency f_0.

(3) The acoustic wave couples to the tuning fork structure, exciting it into resonance.

(4) The oscillations in the tuning fork structure are transduced as an electrical current through the piezoelectric tuning fork.

(5) The tuning fork resonates, re-radiating the acoustic energy.

(6) Viscous damping reduces the amplitude of the tuning fork oscillation and accounts for additional energy loss in the system.

The result is a true multiphysics problem well-suited to modeling with Comsol Multiphysics. The constitutive equations for the system are further described below.

2.1 Light Absorption and Wave Generation

The absorption coefficient, α, is related to species density and spectroscopic characteristics as follows:

$$\alpha = S_{line}(T)\, f_{line}(\nu - \nu_0)\, N \qquad (1)$$

Where $S_{line}(T)$ is the line strength, $f_{line}(\nu-\nu_0)$ is the lineshape function and N is the species density. The line strength and line shape function have been documented for carbon dioxide at a variety of different pressures and temperatures [7].

The acoustic signal then propagates according to the acoustic wave equation:

$$\frac{\partial^2 p(\vec{r},t)}{\partial t^2} - c^2\nabla^2 p(\vec{r},t) = S(\vec{r},t) \qquad (2)$$

Where p is the acoustic pressure, c is the speed of sound, and S is the acoustic source term, which is related to the heat power density deposited in the gas, H, through:

$$S(\vec{r},t) = (\gamma - 1)\frac{\partial H(\vec{r},t)}{\partial t} \qquad (3)$$

In this equation, γ is the adiabatic coefficient of the gas.

The heat power density is related to the absorption coefficient and the laser power density, I (the laser power per unit cross-sectional area of the beam), by:

$$H(\vec{r},t) = \alpha I(\vec{r},t) \qquad (4)$$

For the TFPAS experiments, the beam waist radius is approximately 0.05 mm [6], which is only a quarter of the tuning fork gap (0.2 mm). Therefore, the cross-section of the laser beam is reasonably approximated as a delta function, allowing the source to be modeled as a line through the center of the tuning fork. Thus the heat power density function can be related to the laser power, W as:

$$H(\vec{r},t) = \alpha W \delta^{(2)}(\vec{r})\, e^{i\omega t} \qquad (5)$$

In frequency space, this results in the following wave equation:

$$-\omega^2 p(\vec{r}) - c^2\nabla^2 p(\vec{r}) = i\omega(\gamma - 1)\alpha W \delta^{(2)}(\vec{r}) \qquad (6)$$

Equating this expression to the form of the wave equation used by Comsol, the value for the flow source setting of the line in Comsol is calculated from:

$$\mathrm{iS} = i\frac{(\gamma - 1)\alpha W}{\rho_0 c^2} \qquad (7)$$

This quantity has the units of m^2/s.

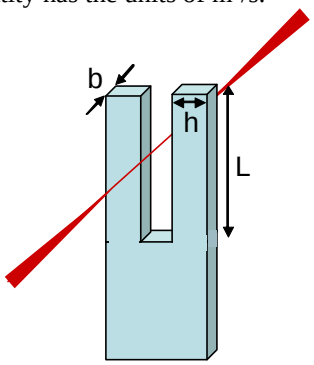

Figure 1. Illustration of the tuning fork structure with incident laser light. The light is modulated at the acoustic resonance of the tuning fork. For the Raltron R38 quartz tuning fork, L = 3.636 mm, h = 0.54 mm and b = 0.232 mm [8]. The gap is 0.2 mm.

2.2 Tuning Fork Response

Figure 1 illustrates the tuning fork structure in relation to the laser beam. The gas of interest surrounds the structure. If the source is modulated at the appropriate frequency, the pressure wave will cause the tuning fork to resonate. The primary resonance frequency can be analytically calculated as the first longitudinal resonance of a cantilever according to [9, 10]:

$$f_0 = \frac{1.015}{2\pi}\frac{h}{L^2}\sqrt{\frac{Y}{\rho_Q}} \qquad (8)$$

Where h is the tine thickness in the direction of motion, L is the tine length, and Y is the Young's modulus and ρ_Q the density of the material (78 GPa and 2650 kg/m^3, respectively, for Quartz [9]). For the dimensions of the Raltron R38

tuning fork, this results in a theoretical resonant frequency of 36 kHz, while the measured resonant frequency is 32.768 kHz. The deviation is mostly due to differences in the nature of the support, which can be addressed in the model geometry.

The mechanical resonance is converted to an electrical signal through the piezoelectric properties of the material. The governing equation for the piezoelectric effect is given by:

$$\vec{D} = d\vec{T} + \varepsilon\vec{E} \quad (9)$$

Where $\vec{D}$ is the polarization vector, d is the piezoelectric coefficient matrix, $\vec{T}$ is the stress vector, ε is the permittivity matrix and $\vec{E}$ is the electric field vector. Thus, mechanical stress results in surface charge on the electrodes, which are on the inner and outer surfaces of the tine. The voltage across the tine is held at zero by the transimpedance amplifier that is used to monitor the current output of the tine. The current output, I_{out}, can be calculated from the surface charge, ρ_s, as follows:

$$I_{out} = \omega \iint \rho_s dA \quad (10)$$

where ω is the radial frequency. Energy loss also occurs within the tuning fork as the result of structural damping and dielectric loss.

2.3 Reradiation

Acoustic radiation is an important energy loss mechanism for the tuning fork [11]. A tuning fork has been shown to act as a linear quadrupole in the plane perpendicular to the fork stem [12]. Therefore it is important that the model include not only the effect of the initial absorption on the tuning fork, but also the motion of the tuning fork on the acoustic field. The total pressure field will be the sum of the quadrupole-like tuning fork pattern and the acoustic wave that results from the initial absorption. Inclusion of the re-radiation is particularly important in analyzing the effect of additional acoustic structures on the system.

2.4 Viscous Damping Effects

Concentration measurements will be conducted at or near atmospheric pressures, where viscous damping plays a significant role in limiting the Q of the resonance [10, 11]. The reaction force resulting from viscous damping on the tuning fork tine can be described as:

$$\vec{F}_r = \beta_1\vec{u} + \beta_2\dot{\vec{u}} \quad (11)$$

Where $\vec{u}$ is the velocity field at the surface of the tine. β_1 captures the resistive portion of the damping, while β_2 captures the inertial or reactive portion.

Blom *et al.* apply the solution for β_1 and β_2 for an oscillating sphere to approximate the damping action of a cantilever, using the sphere radius, R, as a fitting parameter [13]. These parameters are given by [14]:

$$\beta_1 = 6\pi\eta R\left(1+\frac{R}{\delta}\right) \quad (12)$$

$$\beta_2 = 3\pi R^2\sqrt{\frac{2\eta\rho_0}{\omega}}\left(1+\frac{2R}{9\delta}\right) \quad (13)$$

Where η is the dynamic viscosity, ρ_0 is the gas density, ω is the radial frequency, and δ is the boundary layer thickness, given by:

$$\delta = \sqrt{\frac{2\eta}{\rho_0\omega}} \quad (14)$$

For this model, R is fitted to the observed 8 Hz resonant frequency shift observed between operation in vacuum and atmosphere [4]. The drag force, which is pressure dependent through the density, is then added as an implicit damping term on the tine surface in COMSOL. A better damping model might be implemented in future work by coupling in additional COMSOL modules to calculate the damping terms.

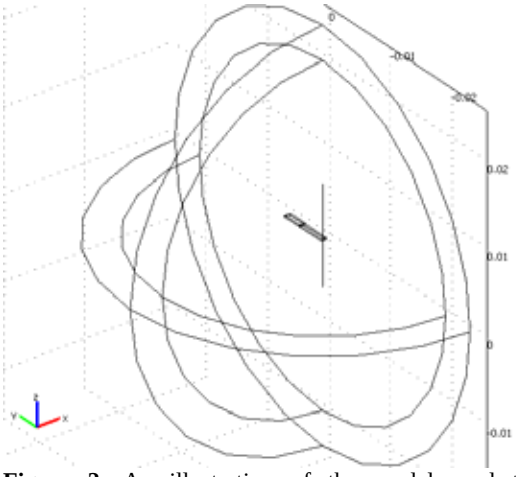

Figure 2. An illustration of the model used to investigate tuning fork PAS behavior.

3. Use of COMSOL Multiphysics

Our model uses the Pressure Acoustics and Piezo Solid segments within the Acoustics

module of COMSOL Multiphysics. In our 3D model, shown in Fig. 2, we take advantage of the symmetry plane along the center axis of the tuning fork. The initial laser power absorption is modeled as a line source through the center of the tuning fork. The line source sets up an acoustic pressure wave that couples mechanically to the tuning fork using a fluid load boundary condition. Because of the anisotropy of the piezoelectric properties, tuning fork alignment to the assumed poling direction in the material properties (the z direction) is critical. This results with the line source in the z direction, and the tuning fork is in the x-y plane with the fork pointed in the y direction.

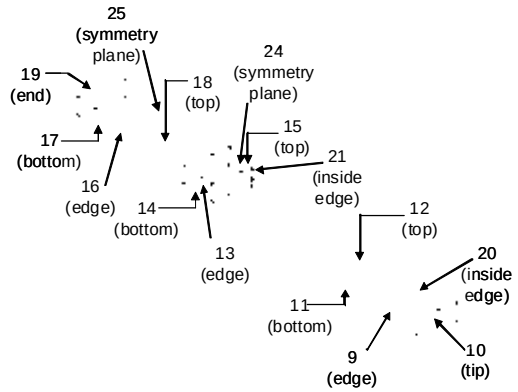

Figure 3. Close up of tuning fork tine with boundaries numbered as they appear in the model.

Only the outer shell and inner sphere subdomains are active in the acoustic subdomain. The outer shell is set up as a spherical perfectly matched layer (PML) to reduce unwanted reflections at the boundary. The tuning fork subdomain is only active in the Piezo Solid domain. The material properties of the tuning fork are taken from the Comsol library entry for quartz. The dielectric loss factor is set at 0.0009, which is the literature value for quartz [15], and the structural loss parameter is set to 9x 10^{-6} to approximately match the observed vacuum Q of the tuning fork [4].

The tuning fork dimensions are those for the Raltron R38 tuning fork, which was used for many of the Rice University experiments. A close up image of the tuning fork structure is shown in Fig. 3 with the surfaces labeled as they appeared in Comsol. The base of the tuning fork is subdivided between fixed and free boundary condition regions to better match the actual structure. The length of the exposed base portion was estimated to be 0.15 mm from [4]. The notch was also rounded with a radius of 0.1 mm to better match the actual structure.

In the acoustics domain, the tine boundaries (9-12, 20, 21) were set at normal acceleration, with the acceleration value set to:

an = nx_smpz3d * u_tt_smpz3d + ny_smpz3d * v_tt_smpz3d + nz_smpz3d * w_tt_smpz3d (15)

The tuning fork stem boundaries (13-19) and outer boundary of the PML shell were set to sound hard boundary conditions.

Table 1. Boundary Settings in Piezo Solid Domain

#s	Constraint	Load	Electric
9, 11, 12, 20	Free	Fx = nx_acpr2*p2-drag Fy = ny_acpr2*p2 Fz = nz_acpr2*p2	Ground
10	Free	Fx = nx_acpr2*p2-drag Fy = ny_acpr2*p2 Fz = nz_acpr2*p2	Zero charge/ symmetry
13-15, 21	Free	0	Zero charge/ symmetry
16-19	Fixed	0	Zero charge/ symmetry
24, 25	Symmetry Plane	0	Zero charge/ symmetry

Table 2. User-Defined Constants

Name	Expression	Description
Freq	32e3 [Hz]	Frequency (varied in parametric study)
E_quartz	7.8e10 [Pa]	Young's modulus for quartz
visc	1.983e-5 [Pa*s]	Dynamic viscosity of air at STP
dens	1.25 [kg/m^3]	Density of air at STP
R	515e-6 [m]	Radius of equivalent sphere for drag force
L	3.636e-3 [m]	Tine length
H	0.54e-3 [m]	Tine width
B	0.232e-3 [m]	Tine thickness

The boundary conditions for the surfaces in the Piezo Solid are as given in Table 1, with the user-defined constants and expressions as given in Tables 2 and 3. The variables "beta1" and "beta2" were defined according to equations (12) and (13). The variable "drag" was created for the tine surfaces (9-12, 20) according to the expression:

drag = (beta1+i*Frad*beta2)*u_t_smpz3d/Area (16)

The output current is calculated using equation (10) on the outer tine surface (boundary 9), as a boundary integration coupling variable.

Table 3. User-Defined Global Expressions

Name	Expression	Description
Frad	2*pi*Freq	Radial frequency
delta	sqrt(2*visc/(dens*Frad)	Boundary layer thickness
Area_ed	L*B	Cross-sectional area of tine edge
Area_fc	L*H	Cross-sectional area of tine face
Area_tp	B*H	Cross-sectional area of tine tip
Area	2*(Area_ed+Area_fc)+Area_tp	Total tine area
beta1	6*pi*visc*R*(1+R/delta)	β_1
beta2	3*pi*R^2*sqrt(2*visc*dens/Frad)*(1+2*R/(9*delta))	β_2

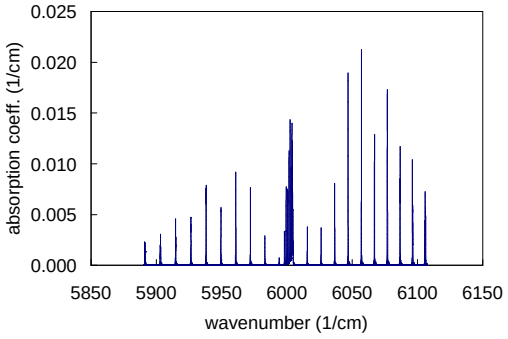

Figure 4. Absorption spectra for CH_4 at 6.7% concentration and 375 Torr. in the wavenumber range of interest.

In order to correlate our model with experimental results in the literature [4, 17], we assume a 2 mW laser operating at the 5999.49 cm^{-1} absorption line of CH_4. (While we are primarily interested in CO_2 measurement, there is less experimental detail given for the CO2 studies). Fig. 4 shows the spectrum of CH_4 in this region at a concentration of 6.7%, and at a pressure of 375 Torr. The spectra assumes room temperature and was calculated from HITRAN data on the Institute for Atmospheric Optics web site [7]. The absorption coefficient at 5999.5 cm^{-1} is $7.73x10^{-3}$ cm^{-1}. The adiabatic coefficient and speed of sound for air is 1.4 and 343 m/s, while the density at 375 Torr is 0.62 kg/m^3. Thus the flow source setting for the edge source using equation (7) should be i*8.5 x 10^{-9} m^2/s.

4. Results

In the absence of viscous damping, the current output as a function of frequency is shown in Fig. 5 below. The resonance frequency for this peak is 32.547 kHz, and the quality factor is 95,726.

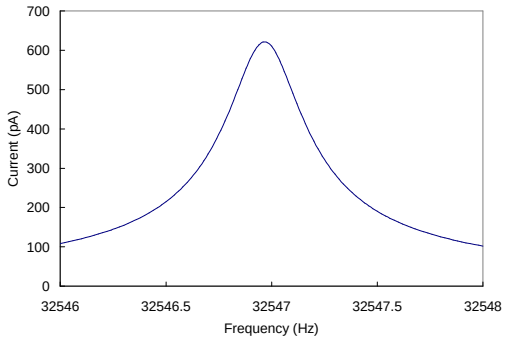

Figure 5. Current as a function of frequency in the absence of viscous damping for 6.7% CH_4 with a 2 mW laser at 5999.49 cm^{-1}.

The quadrupole nature of the acoustic reradiation pattern at tuning fork resonance is visible in the comparison of Fig. 6a, which shows the acoustic field at resonance, to Fig. 6b, which shows the same cross-section off resonance. The effects of damping are illustrated in Fig. 7, which shows the current response with and without the explicit damping terms. The addition of damping reduces the resonance frequency from 32.547 kHz to 32.539 kHz, and the Q from 95,726 to 23,242.

In published experiments, a tuning fork excited by a test voltage yielded a Q of 93,456 and a resonance frequency of about 32.764 kHz in vacuum. At atmosphere, the Q was reduced to 13,271 while the resonance frequency shifted down by 7.5 Hz [4]. The model, therefore, is consistent with the data. The deviation in the resonance frequency is most likely due to differences in the nature of the support, in particular the effective length of the "exposed" base portion which has a free surface boundary condition. For example, when the fork base was modeled entirely with fixed boundary conditions, the modeled resonance frequency was 34.9 kHz, which is in keeping with the resonance predicted by (8).

While the vacuum Q and frequency shift are fitted by the choice of the structural damping term (9 x 10^{-6}) and equivalent sphere radius for viscous damping (515 μm), the resulting Q in the damped model is consistent with the experimental data. Also the fit parameters for the structural damping and equivalent radius are reasonable. For example, the radius calculated by equating the surface area between the tine and the equivalent sphere would be 683 μm, while the radius calculated by equating volume would be 477 μm.

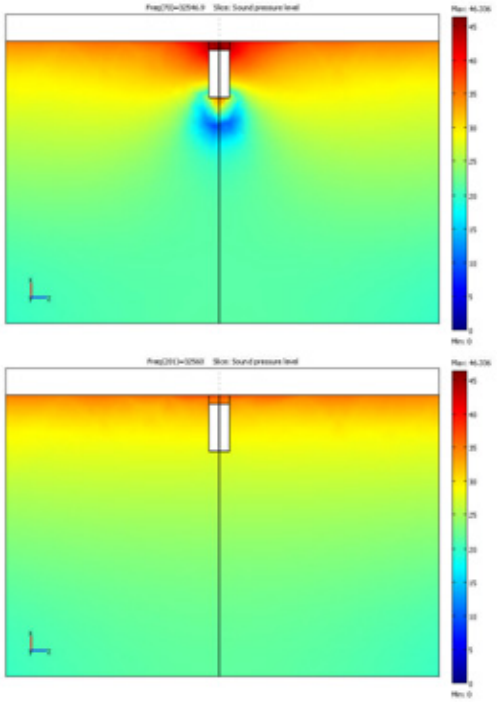

Figure 6. Pressure pattern perpendicular to the tuning fork in the source plane (a) at resonance and (b) off-resonance.

In order to further test our model against experimental data, we applied our model to methane measurement at 375 Torr, matching the conditions in [16], with the density constant adjusted to 0.62 kg/m^3. The R and structural damping factor determined from the above fit were kept the same.

The resulting peak signal was 186 pA. Assuming a 4.4 MΩ feedback resistor, as was used in [16], this results in a voltage signal of 818 μV, or a responsivity of 0.53 V/(W cm^{-1}), when normalizing for laser power and absorption. Kosterev *et al.* [16] achieved a responsivity of 1.24 V/(W/cm) for the same operation condition.

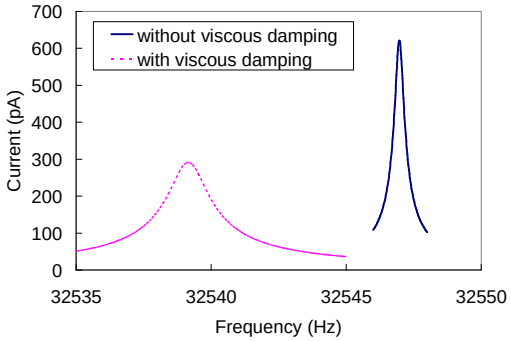

Figure 7. TF response produced by the model for operation with and without damping at atmosphere.

5. Signal Enhancement Studies

We then added resonator tubes to the study in the fashion described by [16] and illustrated in Fig. 8. In [16], these tubes were made from stainless steel tubing and had an outer diameter of 1.59 mm, an inner diameter of 0.51 mm, and a total length, including the gaps around the tuning fork, of 5.3 mm. In our model, we assumed that the tube boundaries were perfectly sound hard.

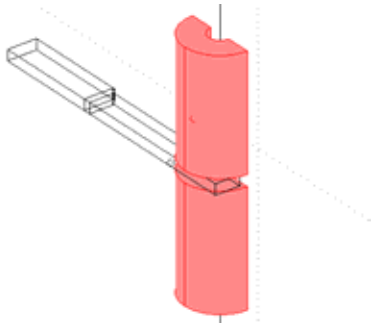

Figure 8. Modeling the effect of adding acoustic resonator structures to the model in the manner described in [16].

The presence of the tubes boosted the responsivity of the system by as much as 50 times, depending on the size of the gaps between the tuning fork and tubes. Our study also revealed the sensitivity of the signal boost on that gap size. Fig. 9 illustrates how a gap of only 50 μm reduced the signal enhancement factor to 15. In experiments, the addition of the acoustic resonator tubes boosted the signal by a factor of 7.6 [16], with the dimensions of the gap not reported. The resonator tubes work by

confining the acoustic energy in the first longitudinal mode of the tube, which is designed to match the resonance frequency of the tuning fork. Therefore, the sensitivity to the gap dimension is to be expected given that the gap represents an acoustic leak very close to the peak pressure point.

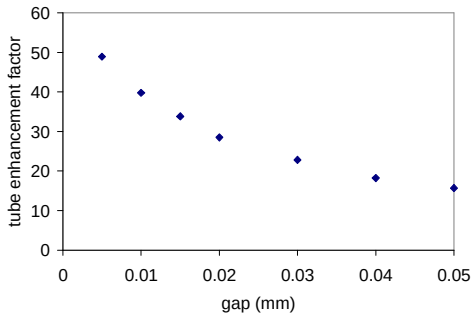

Figure 9. Enhancement to the signal resulting from the presence of the acoustic resonator structure, as a function of the gap between the tubes and the tuning fork.

The modeling supports the conclusion presented by Liu et al. [17] that off-beam positioning of the tuning fork, up against a small slit in the resonator tube results in a greater signal, because this solution allows for a minimal "leak" in the resonator tube.

6. Conclusions

A finite-element model has been developed for a tuning fork photoacoustic spectrometer. The model uses the Pressure Acoustic and Piezo Solid modules in Comsol and includes viscous damping. The results of the model are consistent with experimental results. The model has been used to investigate the addition of acoustic resonator tubes to the system and can be used to test further design options to improve the performance of these sensors.

7. References

1. D. Baldocchi *et al.*, "Measuring Biosphere-Atmosphere Exchanges of Biologically Related Gases with Micrometeorological Methods," *Ecology*, **69**, pp. 1331-1340, (1988).
2. S. Bernegger and M. W. Sigrist, "CO-Laser Photoacoustic Spectroscopy of Gases and Vapours for Trace Gas Analysis," *Infrared Phys.*, **30**, pp. 375-429 (1990).
3. A. Miklos, P. Hess and Z. Bozoki, "Application of Acoustic Resonators in Photoacoustic Trace Gas Analysis and Metrology," *Rev. Sci. Instrum.*, **72**, pp. 1937-1955 (2005).
4. A. Kosterev *et al.*, "Applications of Quartz Tuning Forks in Spectroscopic Gas Sensing," *Rev. Sci. Instrum.*, **76**, 043105.
5. D. Weidmann, *et al.*, "Application of a Widely Electrically Tunable Diode Laser to Chemical Gas Sensing awith Quartz-Enhanced Photacoustic Spectroscopy," Optics Lett., 29, pp. 1837-1839 (2004).
6. N. Petra *et al.*, "Theoretical Analysis of a Quartz-Enhanced Photoacoustic Spectroscopy Sensor," *Appl. Phys. B*, **94**, pp. 673-680, (2009).
7. Institute of Atmospheric Optics, "Spectroscopy of Atmospheric Gases," http://spectra.iao.ru/en/, site accessed Aug. 3, 2009.
8. C. H. Yang *et al.*, "A Low Noise Transimpedance Amplifier for Cryogenically Cooled Quartz Tuning Fork Force Sensors," *Rev. Sci. Instrum.*, 73, 2713 (2002).
9. Y. Qin and R. Reifenberger, "Calibrating a Tuning Fork for Use as a Scanning Probe Microscope Force Sensor," *Rev. Sci. Instrum.*, **78**, 063704, (2007).
10. W. E. Newell, "Miniaturization of Tuning Forks," *Science*, **161**, pp. 1320-1326, (1968).
11. M. Christen, "Air and Gas Damping of Quartz Tuning Forks," *Sensors and Actuators*, **4**, pp. 555-564, (1983).
12. D. A. Russell, "On the Sound Field Radiated by a Tuning Fork," *Am. J. Phys.*, **68**, pp. 1139-1145, (2000).
13. F. R. Blom *et al.*, "Dependence on the Quality Factor of Micromachined Silicon Beam Resonators on Pressure and Geometry," *J. Vac. Sci. Technol. B*, **10**, pp. 19-26, (1992).
14. L. D. Landau and E. M. Lifshitz, *Fluid Mechanics*, Pergamon Press, London, pp. 88-98, 1959.
15. S. C. Leonard and H. H. Race, "Calorimetric Measurement of Dielectric Losses in Solids," Transactions of the American Institute of Electrical Engineers, **55**, pp. 1347-1356, (1936).
16. A. A. Kosterev *et al.*, "Quartz-Enhanced Photoacoustic Spectroscopy," *Optics Lett.*, 27, pp. 1902-1904, (2002).
17. K. Liu *et al.*, "Off-Beam Quartz Enhanced PhotoAcoustic Spectroscopy," to be published in *Optics Letters*.

8. Acknowledgements

Funding for this work was provided by the National Science Foundation (grant number OCE-0852510).